Interactions of Histone H1 with Phospholipids and Comparison of Its Binding to Giant Liposomes and Human Leukemic T Cells†

Hongxia Zhao, Shambhunath Bose, Esa K. J. Tuominen, and Paavo K. J. Kinnunen*,‡

Helsinki Biophysics and Biomembrane Group, Institute of Biomedicine, University of Helsinki, P.O. Box 63, Haartmaninkatu 8, Helsinki FIN-00014, Finland

Received February 3, 2004; Revised Manuscript Received June 7, 2004

ABSTRACT: Due to its net positive charge histone H1 readily associates with liposomes containing acidic phospholipids, such as phosphatidylserine (PS). Interestingly, circular dichroism reveals that while histone H1 in aqueous solutions appears as a random coil, its binding to liposomes containing PS is associated with a pronounced increase in α-helicity and β-sheet content, estimated at 7% and 24%, respectively. This interaction further results in vesicle aggregation and lipid mixing. Fluorescence microscopy revealed rapid binding of Texas Red-labeled H1 (TR-H1) to giant liposomes composed of phosphatidylcholine and PS (SOPC/brain PS, 9/1 molar ratio), followed by lateral segregation and subsequent translocation of the membrane-bound H1 into the giant liposome. The above processes in giant liposomes did depend on the presence of the negatively charged PS. Comparison of the behavior of H1 in giant liposomes to that in cultured leukemic T cells demonstrated very similar patterns. More specifically, fluorescence microscopy revealed binding of TR-H1 to the plasma membrane as lateral segregated microdomains, followed by translocation into the cell. H1 also triggered membrane blebbing and fragmentation of the nuclei of these cells, thus suggesting induction of apoptosis. Our findings indicate that histone H1 and acidic phospholipids form supramolecular aggregates in the plasma membrane of T cells, subsequently resulting in major rearrangements of cellular membranes. Our results allow us to conclude that the minimal requirement for the interaction of histone H1 with the leukemia cell plasma membrane is reproduced by giant liposomes composed of unsaturated phosphatidylcholine and phosphatidylserine, the latter being mandatory for the observed changes in the secondary structure of H1 as well as the macroscopic consequences of the H1−PS interactions.

Conventionally, the functions of histones are connected to the organization of chromatin (*1*). Accordingly, they are crucial for the regulation of gene expression and control changes in nucleosomal packaging of DNA, affecting cell functions, differentiation, and proliferation. The linker histone H1 is essential for the generation of the highly condensed chromatin structure in mammalian cells (*2*). Intriguingly, several studies indicate that the localization of histones is not restricted to the nucleus, thus suggesting that they may perform functions outside the nucleus and also outside the cell (*3*−*7*). Yet, while both histones and DNA are normally present in biological fluids such as serum and milk, their extracellular levels are usually very low, which corresponds very roughly to approximately 0.1 μM histones in serum (*8*). However, under pathological circumstances their concentrations can increase substantially (*9*). Histones have been reported to display hormone-like properties (*10*), and they appear to be involved in autoimmune diseases such as multiple sclerosis, diabetes, and rheumatoid arthritis (*11*, *12*). Apoptotic cells have been found to release significant amounts of histones into the extracellular milieu (*13*). Due to deficient clearance of apoptotic cells in patients with systemic lupus erythematosus (SLE), both nucleosomes and histones accumulate in circulation and have been shown to exert profound effects on cellular functions (*14*, *15*). Histones also represent a phylogenetically very old defense system of the body and disrupt *Escherichia coli* membranes in a manner resembling the action of antimicrobial peptides (*16*). Histone H1 has been suggested to locate at the neuronal cell surface and bind bacterial lipopolysaccharide, a potential inflammogen following systemic infection, arguing for a role for H1 in the defense of the central nervous system against bacteria (*6*). Histones have been found also on the plasma membrane of various cell types (*3*−*7*). Histone H1 has been shown to suppress the growth of leukemia cells, their exposure to H1 resulting in plasma membrane damage (*17*). Histones have been reported to be cytotoxic also to mammalian epithelial cells, increasing cell membrane permeability and leading to cell swelling and, ultimately, to lysis (*18*). The potential extracellular functions of histone H1, especially the effects of H1 on membranes such as mentioned above, are of considerable interest not only because of the possible physiological significance of these interactions but also as a model for the mechanism of action of other cytotoxic cationic proteins.

H1 has been shown to bind avidly to liposomes containing acidic phospholipids (*19*−*21*). We have further demonstrated

† This study was supported by the Finnish Academy. Memphys is supported by the Danish National Research Council.

* Address correspondence to this author. Tel: +358-9-19125400. Fax: +358-9-19125444. E-mail: Paavo.Kinnunen@Helsinki.Fi.

‡ Memphys−Center for Biomembrane Physics.

10.1021/bi049758b CCC: $27.50
Published on Web 07/16/2004

that H1, DNA, and liposomes containing acidic phospholipids form ternary complexes (*20*). The affinity of H1 to negatively charged lipids is very high, far exceeding that of cytochrome *c* (*21*, *22*). These observations are intriguing as H1 is generally not considered to be a peripheral membrane protein, in contrast to cytochrome *c*. Possible roles of lipids (*20*) in the biological activities of histones remain unknown. The cytotoxic activity of H1 has been suggested to be due to channel formation in membranes, this process being enhanced by anionic phospholipids (*18*). Interaction of H1 with phosphatidylserine (PS)[1] is known to be involved in coagulation disorders. In brief, the exposure of the anionic procoagulant phospholipid, PS, on the cell surface is needed for blood coagulation (*23*), and it is rapidly released during cell injury (*19*). Patients with anti-phospholipid syndrome, SLE, and drug-induced SLE have both anti-histone and anti-phospholipid antibodies (*14*). Histone H1 prolongs and anti-H1 antibodies significantly shorten the clotting time, indicating that H1 acts as an anticoagulant (*24*). This effect has been suggested to be due to scavenging of PS by H1, thus preventing the activation of the coagulation cascade by PS (*19*, *20*), and bears clinical significance regarding autoimmune syndromes and anti-histone antibodies, where anti-H1 may inhibit the histone−phospholipid interaction and predispose these patients to thrombosis (*25*).

The binding of histone H1 to phosphatidylcholine liposomes both with and without PS as well as changes in the secondary structure of H1 in different environments was investigated. Intriguingly, a significant increase in α-helicity and *β*-sheet structure of H1 was induced in the presence of liposomes containing the anionic phospholipid, PS. In contrast, H1 remained structureless in the presence of neutral membranes composed of phosphatidylcholine. H1 also caused pronounced aggregation and fusion of anionic phospholipid containing membranes with minor effects on neutral membranes. Subsequently, we investigated the topological consequences induced by H1 in model biomembranes and compared these with the processes involved in the cytotoxic effects of histone H1 on leukemic T cells. More specifically, the interaction of H1 with plasma membrane was modeled using giant liposomes. The latter membranes have diameters comparable to most eukaryotic cells, thus enabling the characterization of individual vesicles in real time using microscopy techniques. Following microinjection of TR-H1 onto the vesicle surface aggregation of histone H1 on the liposome, domain formation, and translocation of the H1-induced domains as vesicles shedding from the vesicle bilayer into the internal cavity of the giant liposome were evident.

The binding of histone H1 to leukemic T cells caused similar and profound changes in their plasma membrane morphology, with rapid binding of H1 and aggregation of the membrane-associated H1. These surface-aggregated domains enriched in H1 subsequently translocated into the cells following very similar patterns as observed for the binding of H1 to individual, isolated giant liposomes. The data presented here also indicate histone H1 to induce apoptosis of cultured human leukemic T cells. Because of the above changes in the involved structures on various time and length scales (from molecular dynamics to microscopy), the membrane is unlikely to maintain its normal function as a selective permeability barrier. We conclude the binding of histone H1 to acidic phospholipids to involve substantial lateral lipid demixing, followed by the formation of supramolecular aggregates and their cusping in the cell membrane, with subsequent shedding of these structures into the cell, eventually triggering apoptosis.

EXPERIMENTAL PROCEDURES

Materials. Brain phosphatidylserine (brain PS), 1-stearoyl-2-oleoyl-*sn*-glycero-3-phosphocholine (SOPC), 1-palmitoyl-2-[[(*N*-4-nitrobenz-2-oxa-1,3-diazolyl)amino]caproyl]-*sn*-glycero-3-phosphocholine (NBD-PC), L-α-1,2-dipalmitoyl-*sn*-glycero-3-phospho[*N*-(4-nitrobenz-2-oxa-1,3-diazolyl)]-ethanolamine (DPPN), and 1,2-dioleoyl-*sn*-glycero-3-phosphoethanolamine-*N*-(lissamine rhodamine B sulfonyl) (DOPRho) were from Avanti Polar Lipids (Alabaster, AL). Hoechst 33342 and sytox green nucleic acid stain (5.0 mM in DMSO) were from Molecular Probes (Eugene, OR). The purity of the above lipids was checked by thin-layer chromatography on silicic acid coated plates (Merck, Darmstadt, Germany) developed with chloroform/methanol/water (65:25:4 v/v/v). Examination of the plates after iodine staining and, when appropriate, upon UV illumination revealed no impurities. Other chemicals were of analytical grade from standard sources. The concentrations of fluorescent lipids were determined spectrophotometrically using the molar absorptivities $\epsilon_{463} = 21000\ M^{-1}\ cm^{-1}$ (in CH_3OH), $\epsilon_{465} = 19000\ M^{-1}\ cm^{-1}$ (in C_2H_5OH), and $\epsilon_{560} = 75000\ M^{-1}\ cm^{-1}$ (in CH_3OH) for DPPN, NBD-PC, and DOPRho, respectively. Concentrations of the nonfluorescent lipids were determined gravimetrically with a high-precision electrobalance (Cahn, Cerritos, CA).

Labeling of Histone H1. H1 was either purified from calf thymus essentially as described previously (*26*) or purchased from Upstate (Lake Placid, NY; purity >95%) and labeled with the FluoReporter Texas Red-X protein labeling kit (Molecular Probes, Leiden, The Netherlands). The degree of labeling amounted to 1.0−2.0 bound dye molecules per H1.

Preparation of Large and Small Unilamellar Vesicles. Appropriate amounts of the lipid stock solutions were mixed in chloroform to obtain the desired compositions. The solvent was removed under a stream of nitrogen, and the lipid residue was subsequently maintained under reduced pressure for at least 2 h. The dry lipids were then hydrated at 50 °C in 5 mM Hepes, 0.1 mM EDTA, and 150 mM NaCl, pH 7.4. The resulting dispersions were extruded through a single polycarbonate filter (100 nm pore size; Millipore, Bedford, MA) using a Liposofast low-pressure homogenizer (Avestin,

[1] Abbreviations: brain PS, brain phosphatidylserine; CD, circular dichroism; DEF, DNA fragmentation factor; DIC, differential interference contrast; I_1, fluorescence emission through a polarizer parallel to polarized excitation; I_2, fluorescence emission through a polarizer perpendicular to polarized excitation; LUVs, large unilamellar vesicles; PS, phosphatidylserine; SOPC, 1-stearoyl-2-oleoyl-*sn*-glycero-3-phosphocholine; NBD-PC, 1-palmitoyl-2-[[(*N*-4-nitrobenz-2-oxa-1,3-diazolyl)amino]caproyl]-*sn*-glycero-3-phosphocholine; DPPN, L-α-1,2-dipalmitoyl-*sn*-glycero-3-phospho[*N*-(4-nitrobenz-2-oxa-1,3-diazolyl)]-ethanolamine; DOPRho, 1,2-dioleoyl-*sn*-glycero-3-phosphoethanolamine-*N*-(lissamine rhodamine B sulfonyl); SUVs, small unilamellar vesicles; TR-H1, Texas Red-labeled histone H1; *X*, mole fraction of the indicated lipid.

Ottawa, Canada) to obtain large unilamellar vesicles (LUVs) with average diameters between 111 and 117 nm (*27*). Small unilamellar vesicles (SUVs) with an average diameter of approximately 26.5 nm were formed by ethanol injection essentially as described by Batzri and Korn (*28*).

Binding of Histone H1 to Large Unilamellar Vesicles. Binding of H1 to liposomes was monitored by measuring fluorescence anisotropy (r) for Texas Red-labeled histone H1 (TR-H1) as well as using resonance energy transfer. In the former assay a Perkin-Elmer LS 50B spectrofluorometer was employed with polarized excitation at 595 nm and emission at 615 nm, using 10 nm bandwidths. The values for r were calculated according to the equation:

$$r = (I_1 - I_2)/(I_1 + 2I_2)$$

where I_1 and I_2 represent fluorescence intensities with the emission polarizer parallel and perpendicular, respectively, to the polarized excitation (*29*). The concentration of TR-H1 in the assay was 0.6 μM while the content of LUVs was varied as indicated and is given as the concentration of phospholipids.

For the measurement of resonance energy transfer NBD-PC ($X = 0.02$) was included in the liposomes as a donor, and its fluorescence was monitored with excitation at 460 nm and emission at 520 nm, using 10 nm bandwidths, while varying the concentration of TR-H1 (acceptor). The total concentration of phospholipids was 20 μM with temperature maintained at 25 °C.

Recording Circular Dichroic Spectra. UV region (from 250 to 190 nm) spectra for histone H1 were recorded with a CD spectrophotometer (Olis RSF 1000F; On-line Instrument Systems Inc., Bogart, GA) with the cuvette temperature maintained at 25 °C using a circulating water bath. Spectra were measured in H_2O and 10%, 30%, and 50% trifluoroethanol as well as in the presence of small unilamellar vesicles (SUVs). The concentration of histone H1 in H_2O and trifluoroethanol was 9 μM whereas 2 μM H1 was used in the presence of 400 μM SUVs. A 1 mm path length quartz cell was used, and interference by circular differential scattering by liposomes was eliminated by subtracting the CD spectra for liposomes from those recorded in the presence of histone H1. Data shown represent the averages of six scans. Estimates of the protein secondary structures were derived from the CD spectra using the K2d program (*30*).

Measurement of Light Scattering. Intensity of 90° light scattering of the liposomes was monitored at 500 nm using the Perkin-Elmer LS 50B spectrofluorometer with both excitation and emission bandwidths set at 2.5 nm. Scattering intensity was measured continuously after the addition of 60 nM histone H1. The lipid concentration was 40 μM. Otherwise, conditions were as in the fluorescence measurements. Scattering of the buffer solution with or without histone H1 in the absence of LUVs was negligible.

Assay for Lipid Mixing. LUVs labeled with DPPN ($X = 0.02$) were mixed at 1:1 ratio with LUVs containing DOPRho ($X = 0.02$). Intermixing of the lipids of the two vesicle populations leads to resonance energy transfer from Nbd (donor) to rhodamine (receptor) and thus results in a decrease in Nbd emission. Fluorescence of Nbd was measured continuously using excitation at 460 nm and emission at 520 nm, with 10 nm bandwidths. The total phospholipid concentration was 40 μM, and the amount of H1 added was as indicated. The assay was conducted at a temperature of 25 °C maintained in the cuvette compartment with a circulating water bath.

Formation of Giant Liposomes. Giant liposomes were prepared as described elsewhere (*31*−*34*). Approximately 2−4 μL of the indicated lipids dissolved in diethyl ether/methanol (9:1 v/v, at a concentration of 1 mM) was applied onto the surface of the two Pt electrodes and subsequently dried under a stream of nitrogen. Possible residues of the organic solvents were removed by evacuation in a vacuum for 1 h. A glass chamber with the attached electrodes and a quartz window bottom was placed on the stage of an Olympus IX 70 inverted fluorescence microscope. An AC field (sinusoidal wave function with a frequency of 8 Hz and amplitude of 0.2 V) was applied before 2 mL of 0.5 mM Hepes buffer, pH 7.4, was added. During the first minute of hydration the voltage was increased to 2 V. The AC field was turned off after 2 h, and giant liposomes were observed with differential interference contrast (DIC) optics with a 20/0.40 objective. The diameters of giant liposomes were measured using calibration of the images by motion of the micropipet as proper multiples of the step length (50 nm) of the micromanipulator (MX831 with MC2000 controller; SD Instruments, Grants Pass, OR) and were found to vary between 10 and 500 μm. Images were recorded with a Peltier-cooled 12-bit digital CCD camera (C4742-95; Hamamatsu, Hamamatsu City, Japan) interfaced to a computer and operated by the software (HiPic 5.0.1 or Aquacosmos 1.2) provided by the camera manufacturer.

Micromanipulation. Micropipets were drawn from borosilicate capillaries (1.2 mm outer diameter) by a microprocessor-controlled horizontal puller (P-87; Sutter Instrument Co., Novato, CA). Cells in culture medium (see below) were transferred into a glass chamber (i.d. = 2.5 cm, volume = 2 mL) with a quartz window bottom and were immobilized for the experiments by holding them by a micropipet (tip diameter $\approx$ 5 μm) using a slight negative pressure of the pneumatic microinjector (PLI-100; Medical Systems Corp., Greenvale, NY). Subsequently, the cell culture medium was replaced with PBS while maintaining the cell immersed into the liquid and avoiding its exposure to air. Indicated amounts of 0.2 mM histone H1 were applied onto the cells or the surface of individual giant liposomes as a series of single injections of approximately 20 fL each (corresponding to approximately 4 amol each) and delivered with the PLI-100 pneumatic microinjector. For easier handling only vesicles attached to the electrode surface were used. All experiments were performed at ambient temperature ($\approx$+24 °C).

Confocal Fluorescence Microscopy. An inverted microscope (Olympus IX 70; Olympus Optical Co., Tokyo, Japan) was employed with a confocal scanner (Yokogawa, Tokyo, Japan) and a krypton ion laser (Melles Griot, Carlsbad, CA) as a light source, with excitation (488 and 568 nm) and long-pass emission filter sets appropriate for monitoring Texas Red and sytox green fluorescence. Epifluorescence studies were carried out with the same microscope with an 100 W mercury vapor lamp for epiillumination, and the excitation and emission filter sets were BP 520−550 and LP 580 for Texas Red and BP 365 $\pm$ 50 and BP 450 $\pm$ 58 for Hoechst. Images were acquired with a B/W CCD camera (C4742-95-12 NRB; Hamamatsu Photonics K. K., Hamamatsu,

Japan) interfaced to a computer and operated by the software (AquaCosmos) provided by the camera manufacturer.

Cell Cultures. Human leukemia T cells (Jurkat) were grown in a completely humified atmosphere with 5% CO_2 at 37 °C in RPMI-1640 medium (Gibco, Paisley, U.K.), supplemented with 10% fetal bovine serum, penicillin (100 units/mL), streptomycin (100 μg/mL), and amphotericin B (0.25 μg/mL; Gibco). Cell viability was checked with trypan blue exclusion.

Approximately 1.5×10^6 cells/mL were used for each assay. The cells were washed three times with PBS, and the cell pellet was subsequently resuspended in the same buffer. Both sytox green and Hoechst 33324 were used for staining, as follows. To check cell viability following their exposure to 2.3 and 4.6 μM TR-H1, 50 μM sytox green staining solution in PBS was added to a final concentration of 0.5 μM. In complementary series of experiments 10.7 μM Hoechst 33342 was added along with TR-H1 to monitor H1 binding and the nuclear characteristics simultaneously. Control cells were supplemented with the same volume of PBS in the absence of TR-H1 and stained either with sytox green or with Hoechst 33342. The cells were incubated at 37 °C in a water bath for 30 min in dark, followed by three washing steps with PBS. The cells were finally resuspended in PBS and observed by fluorescence microscopy.

RESULTS

Binding of Histone H1 to Liposomes. Binding of H1 to PC as well as PS/PC liposomes was first assessed by monitoring changes in the emission anisotropy (r) of the Texas Red-labeled H1 resulting from its association to vesicles. While the value for r for the fluorophore moiety of TR-H1 did increase in the presence of PC liposomes (Figure 1, panel A), this increment was more pronounced when the anionic phospholipid PS was present in the membranes. These data are in keeping with a preferential binding of H1 to membranes containing negatively charged phospholipids, as reported previously (*19*−*22*). Resonance energy transfer experiments showed a similar pattern, with significant decrease in fluorescence of the Nbd-labeled phospholipid (DPPN, donor) in liposomes due to energy transfer to the Texas Red-labeled histone H1 (acceptor, Figure 1, panel B). The binding was augmented for membranes containing PS ($X = 0.2$), with maximally approximately 85% decrement in donor fluorescence intensity in the presence of 0.46 μM TR-H1, corresponding to a H1:phospholipid stoichiometry of 1:43.

Secondary Structure of Histone H1. Subsequently to the above experiments revealing enhanced binding of H1 to liposomes containing the acidic phospholipid, phosphatidylserine, we investigated possible lipid-induced changes in the secondary structure of H1 by measuring CD spectra. The single minimum at approximately 198 nm seen for H1 in an aqueous solution indicates the protein to be a random coil (Figure 2). In the presence of neutral membranes composed of phosphatidylcholine the secondary structure of histone H1 remained disordered (Figure 2, panel B). Importantly, a pronounced increase in the content of α-helicity and β-sheet in H1 structure, up to 7% and 24% (Table 1), respectively, became evident upon the binding of H1 to membranes containing the acidic phospholipid PS (Figure 2, panel B).

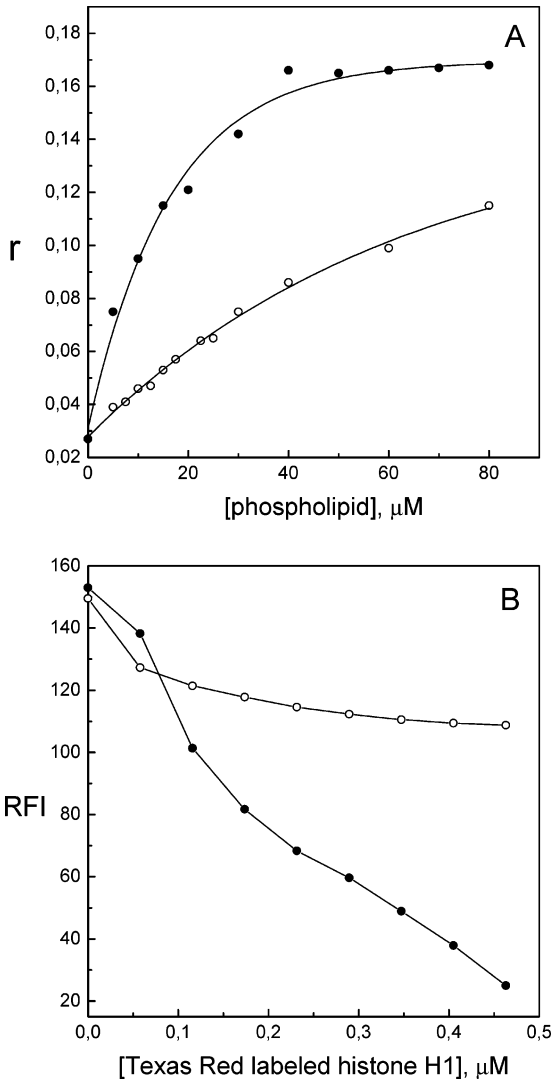

FIGURE 1: Binding of histone H1 to liposomes assessed by fluorescence anisotropy for Texas Red-labeled histone H1 upon the addition of increasing concentrations of liposomes (panel A) and resonance energy transfer from NBD-PC to Texas Red-labeled H1, monitored by a decrease in NBD fluorescence (panel B). The concentrations of histone H1 (panel A) and lipids (panel B) were 0.6 and 20 μM, respectively. The lipid compositions were SOPC (○) and SOPC/brain PS ($X_{PS} = 0.2$, ●). Each data point represents the mean of triplicate measurements. The standard deviations were not shown for the sake of clarity.

Likewise, CD spectra recorded in the presence of increasing concentrations of trifluoroethanol (Figure 2, panel A) suggest a progressive increase in its α-helicity as well as β-sheet structure (*30*). Accordingly, both electrostatic and hydrophobic interactions could be involved in the binding of H1 to PS/PC liposomes, causing changes in the secondary structure of this protein.

Aggregation, Fusion, and Rupture of Vesicles Induced by Histone H1. Possible morphological transformation of vesicles due to histone H1 was studied by light scattering at 90°. The scattering intensity remained unchanged and became noisy upon the addition of histone H1 to SOPC vesicles, suggesting that H1 could weakly and reversibly bind to the SOPC vesicle surface (Figure 3, panel A). However, for LUVs containing the anionic PS scattering first increased, in keeping with binding of H1 to the LUVs (*35*). Subsequently, a point was reached where scattering decreased

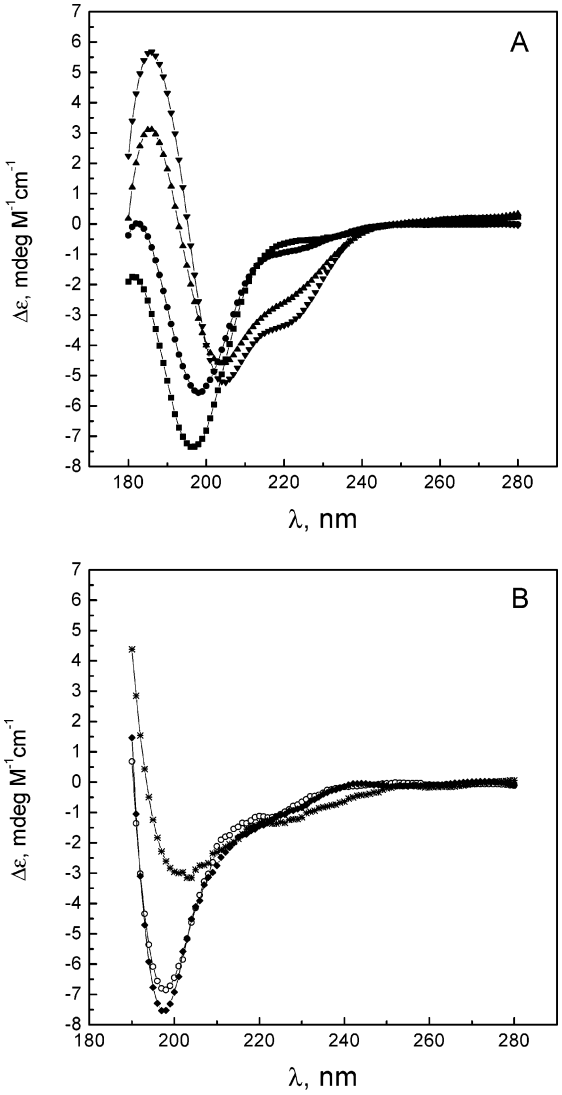

FIGURE 2: Circular dichroic spectra of histone H1 measured in H_2O (■) and in 10% (●), 30% (▲), and 50% (▼) (by volume) trifluoroethanol (panel A), as well as in 5 mM Hepes and 0.1 mM EDTA, pH 7.4 (◆), and in the presence of small unilamellar vesicles (total lipid concentration was 400 μM, panel B) composed of SOPC with $X_{PS} = 0$ (○) and $X_{PS} = 0.2$ (*). The concentrations of histone H1 were 9 (panel A) and 2 μM (panel B). The calculated percentages of α-helix, β-sheet, and random coil for these spectra are compiled in Table 1.

Table 1: Calculated Percentages of α-Helix, β-Sheet, and Random Coil Estimated from the CD Spectra Depicted in Figure 2[a]

	α-helix (%)	β-sheet (%)	random coil (%)
H_2O	2	11	87
10% TFE	4	31	65
30% TFE	28	30	43
50% TFE	28	30	42
SOPC	7	17	76
SOPC/brain PS (8/2)	9	35	56

[a] See text for details.

rapidly below the starting level (Figure 3, panel A), implying rupture and macroscopic aggregation of the vesicles (*36*, *37*). Large aggregates were observed at this point also by visual inspection.

The possibility that histone H1 would cause aggregation and/or fusion of LUVs was investigated using lipid mixing assay (*38*). In the absence of histone H1, Nbd fluorescence

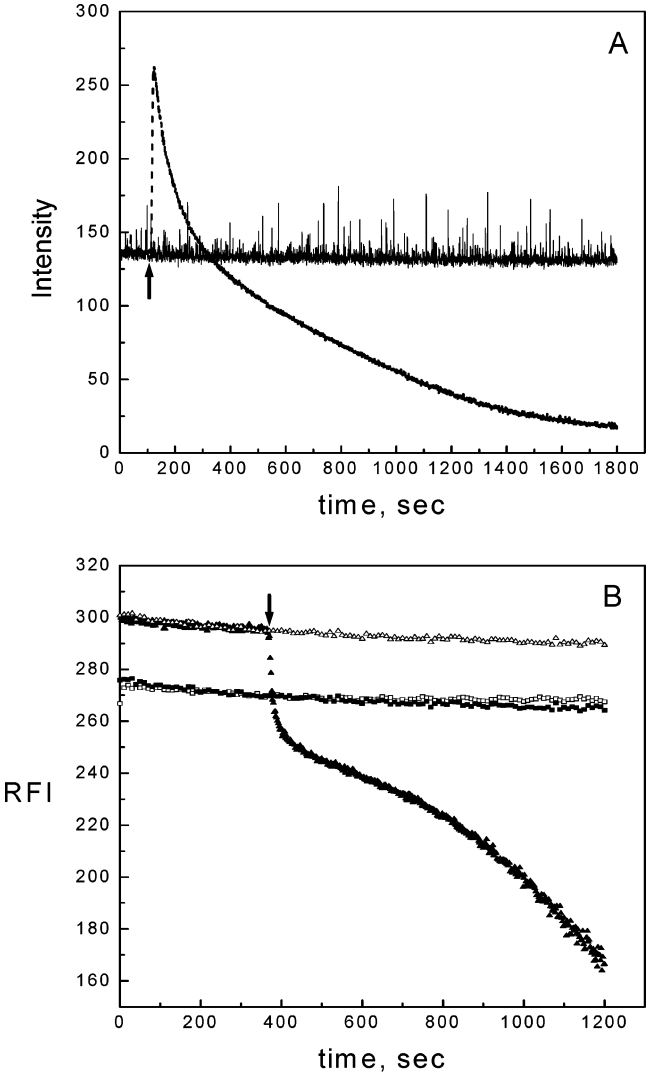

FIGURE 3: Aggregation and fusion of liposomes by H1 revealed by 90° light scattering (panel A) and lipid mixing (final concentration of H1 was 0.06 μM) in 40 μM LUVs (panel B). The lipid compositions were SOPC (—) and SOPC/brain PS (X_{PS} = 0.2, ---). In the lipid mixing assay (panel B), two groups of LUVs labeled with DPPN ($X = 0.02$) and DOPRho ($X = 0.02$) were mixed at a 1:1 ratio both in the absence (□, SOPC) (△, SOPC/brain PS, $X_{PS} = 0.2$) and in the presence (■, SOPC) (▲, SOPC/brain PS, X_{PS} = 0.2) of histone H1. Each data point represents the mean of triplicate measurements. The standard deviations were not shown for the sake of clarity. The arrows show the addition of histone H1.

decreased slightly upon the mixing of two populations of LUVs labeled with DPPN ($X = 0.02$) and DOPRho (X = 0.02) at a 1:1 ratio, respectively. This decrement could be due to contacts between the two groups of labeled vesicles (Figure 3, panel B). For SOPC LUVs, the addition of histone H1 caused only insignificant changes in DPPN fluorescence compared to the control, suggesting that vesicle aggregation did not occur. However, for SOPC liposomes containing the negatively charged phospholipid PS ($X = 0.2$) the addition of H1 caused a rapid decrease in Nbd emission (Figure 3, panel B), revealing aggregation and/or fusion of the vesicles to be triggered by histone H1, with lipid mixing.

Macroscopic Changes in Giant Liposomes Caused by Histone H1. Following the above experiments on small liposomes, we investigated the more macroscopic conse-

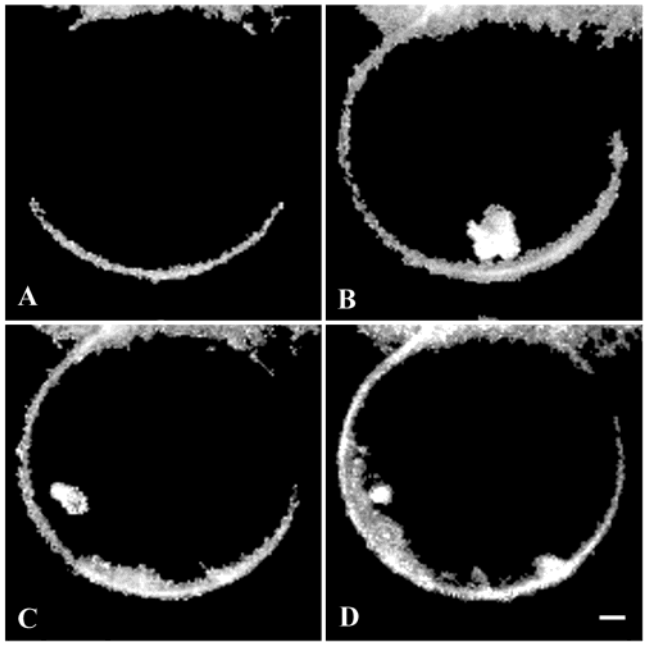

FIGURE 4: Binding of Texas Red-labeled histone H1 to a single SOPC/brain PS (9:1 molar ratio) giant liposome. Fluorescence microscopy images were taken 10 s after the addition of ≈67 amol (panel A), 5 s after the addition of 74 amol (panel B), 10 s after the addition of 82 amol (panel C), and 15 s after the addition of 100 amol (panel D) of TR-H1. Magnification is 20×, and the length of the scale bar (panel D) corresponds to 10 μm.

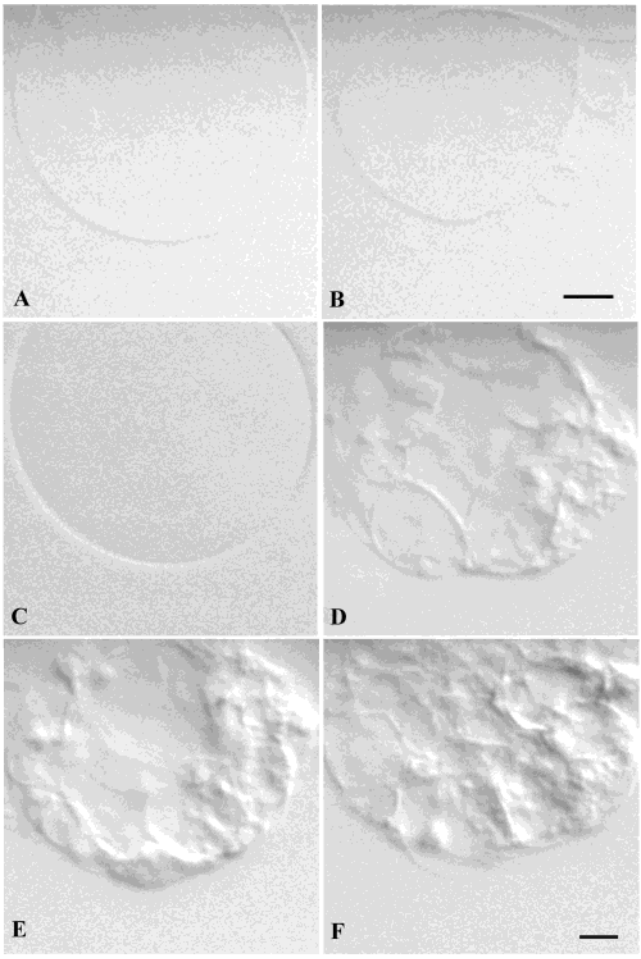

FIGURE 5: DIC images depicting the morphological transformation of giant liposomes caused by histone H1. SOPC giant vesicle before (panel A) and 2 s after the addition of ≈0.4 fmol of histone H1 (panel B). SOPC/brain PS ($X_{PS} = 0.1$) giant vesicle before (panel C) and immediately after the addition of ≈20 amol (panel D), 60 amol (panel E), and 160 amol (panel F) of histone H1. Magnification is 20×, and the length of the scale bars in panels B and F corresponds to 10 μm.

quences of the interactions of H1 with lipids using giant vesicles. The latter represent an interesting and novel type of model biomembrane (e.g., refs *32*, *33*, and *39*−*41*). To observe the binding and distribution of histone H1 in the membranes, Texas Red-labeled histone H1 was applied from a micropipet onto the outer surface of individual giant liposomes, without contacting neighboring vesicles so as to avoid aggregation. To promote the electrostatic association of H1 with giant vesicles, PS was included ($X_{PS} = 0.1$) in the giant vesicles. For these liposomes containing PS, the addition of approximately 67 amol of TR-H1 on the surface of the vesicle caused an intense fluorescence of the giant vesicle membrane, in keeping with the binding of histone H1 to the surface (Figure 4, panel A). Subsequent aggregation of H1 on the membrane surface became evident after the addition of approximately 74 amol (total amount) of TR-H1, and within ≈5 s this aggregate transferred into the giant liposome (Figure 4, panel B). The clustering of TR-H1 on the membrane surface was augmented upon further addition of histone H1 (total amount added being approximately 82 amol), with the area of the brightly fluorescent domain increasing (Figure 4, panel C). When the total amount of H1 injected was increased to ≈100 amol, more aggregates were observed to translocate into the giant liposome (Figure 4, panel D).

In keeping with only a weak interaction between H1 and vesicles composed of the zwitterionic phosphatidylcholine SOPC, giant liposomes remained unaffected until approximately 0.3 fmol of histone H1 was added on the surface of the membrane (data not shown). However, shrinkage and vesiculation of the giant liposomes became evident when the SOPC liposomes were exposed to higher amounts of the protein (approximately 0.4 fmol, 80 repeated injections; Figure 5, panel B). However, the pattern described above for PS containing giant liposomes was not observed; viz., aggregation of TR-H1 on the vesicle surface and translocation into the giant liposomes were not seen (data not shown).

Interestingly, in the presence of PS ($X = 0.1$), pronounced and rapid effects of histone H1 on contacting vesicles became evident. More specifically, aggregation and fusion of such vesicles was caused by histone H1 (Figure 5, panels D−F). Upon the addition of ≈20 amol of H1 on the surface of the giant liposome, the neighboring vesicles started to aggregate with the target liposome (Figure 5, panel D). Further addition of histone H1 (≈60 amol) induced more pronounced and dense aggregates (Figure 5, panel E). Fusion of nearby smaller vesicles and their collapse were observed when approximately 160 amol of H1 had been applied on the surface of the giant liposome (Figure 5, panel F). This effect of histone H1 could be visualized also by fluorescence microscopy for giant liposomes containing the fluorescent lipid probe, NBD-PC (data not shown). Subsequently, we studied the clustering of histone H1 in the course of vesicle aggregation and fusion by monitoring TR-H1 on the surface of a giant liposome ($X_{PS} = 0.1$) with contacting neighboring

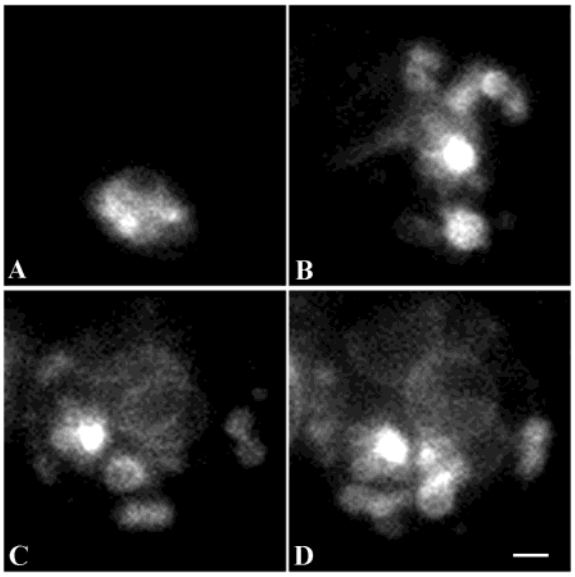

FIGURE 6: Binding of Texas Red-labeled histone H1 to SOPC/brain PS (9:1 molar ratio) giant liposomes. Fluorescence microscopy images were taken immediately after the addition of ≈50 amol (panel A), 90 amol (panel B), 110 amol (panel C), and 130 amol (panel D) of TR-H1. Magnification is 20×, and the length of the scale bar (panel D) corresponds to 10 μm.

vesicles. The liposomes became visible, and similar to the observations reported above, a vigorous aggregation of TR-H1 and vesicles was evident for the acidic phospholipid containing membranes. Fusion of neighboring vesicles as well as translocation of TR-H1 and lipid aggregates into the internal cavity of giant liposomes was evident (Figure 6).

Binding of Histone H1 to Human Leukemic T Cells. Histone H1 has been previously shown to be toxic to mammalian leukemia and epithelial cells (*17*, *18*). We observed the addition of H1 (2.3 and 4.6 μM final concentrations) to human leukemic T cells in suspension to cause the typical morphological hallmarks of apoptosis, i.e., plasma membrane blebbing as well as condensation and fragmentation of their nuclei (data not shown). To study the fate of the added H1 in these cells, we used H1 labeled with Texas Red. TR-H1 bound avidly to the surface of cultured leukemic T cells (Figure 7, panel A), and it was also observed in the intracellular space. Examination at higher magnification revealed a distinct ring of intense peripheral fluorescence in the majority of the cells (Figure 8, panels A1 and A4), suggesting binding of TR-H1 to the plasma membrane. Most cells exhibited a heterogeneous and punctate fluorescence, in keeping with the aggregation of the membrane-bound H1 or its binding to existing microdomains. Sytox green counterstaining showed approximately 12% cell necrosis after exposure of the cells to 4.6 μM TR-H1 (Figure 7, panels A and B). H1 induced plasma membrane blebbing and fragmentation of nuclei in many of the cells, essentially identically to cells treated with the unlabeled H1. Interestingly, the nuclei of some apoptotic cells were intensively stained with TR-H1, and it appeared that these nuclei were also more condensed than those in cells without the accumulation of TR-H1 (Figure 8, panels 6−8). A very similar binding pattern was seen for dead cells with their nuclei concentrating TR-H1 (data not shown). In some experiments individual cells attached to a micropipet were employed, and H1 was added onto their surface by microinjection (Figure 9, panel C). In these cells a similar binding pattern of TR-H1 to the plasma membrane and translocation of the aggregates into the cells were found as described above for cells in suspension (Figure 9).

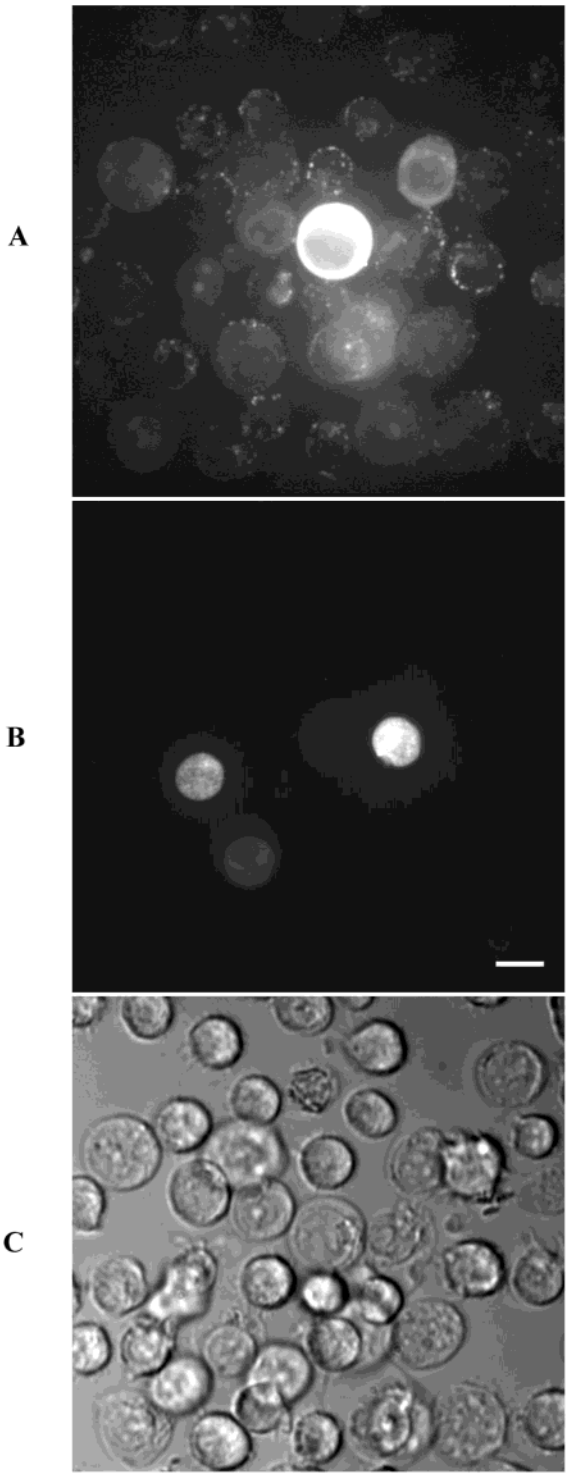

FIGURE 7: Binding of Texas Red-labeled histone H1 (TR-H1) to leukemic T cells. Panels A and B are confocal images of cells stained with 4.6 μM TR-H1 (A) and sytox green (B). Panel C shows a DIC image of the same cells. Magnification is 60×, and the length of the scale bar (panel B) corresponds to 10 μm.

DISCUSSION

Our data here confirm results from our own previous studies as well as those from other laboratories demonstrating

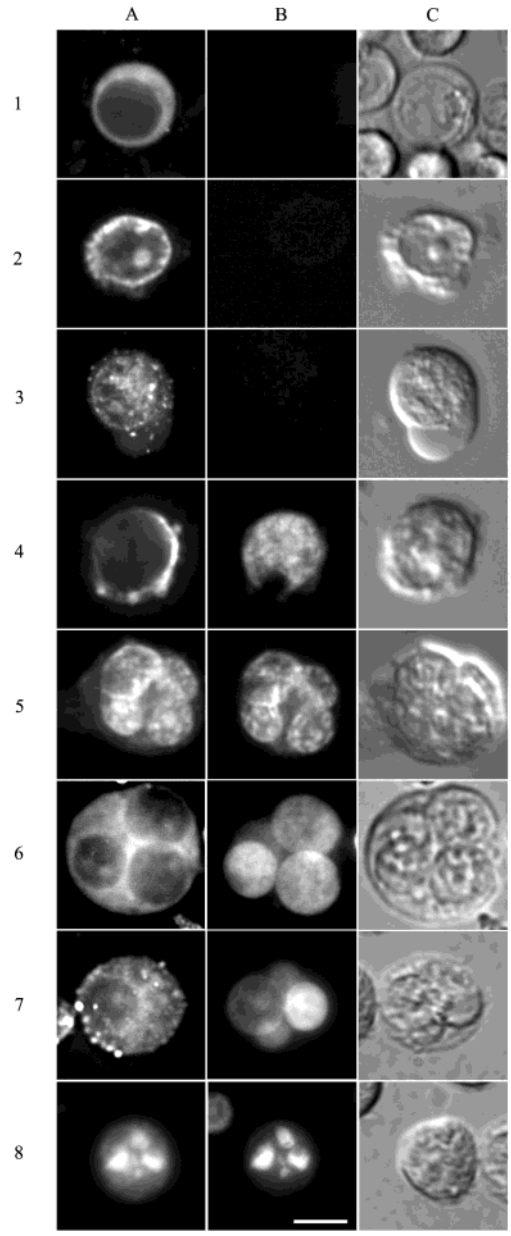

FIGURE 8: Binding of Texas Red-labeled histone H1 (TR-H1) to leukemic T cells. The vertical columns are confocal images of cells stained with (column A) 4.6 μM (1−5) or 2.3 μM (6−8) TR-H1 and (column B) sytox green (1−5) or Hoechst 33324 (6−8). Column C shows DIC images of the same cells. Magnification is 90×, and the length of the scale bar (panel B) corresponds to 10 μm.

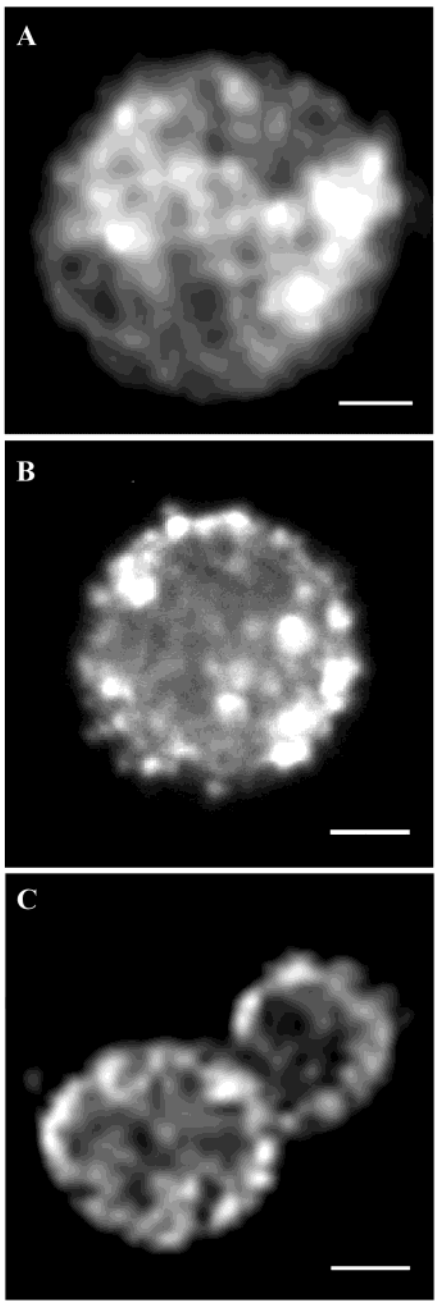

FIGURE 9: Comparison of the patterns of TR-H1 in a giant liposome (SOPC/brain PS, molar ratio 9:1, panel A) and in leukemic T cells either in suspension (panel B) or held with a micropipet (panel C). The total amount of TR-H1 was 0.5 or 0.7 fmol, added by local microinjection onto the giant vesicle or plasma membrane surfaces (panels A and C), respectively. In panel B, the final concentration of H1 was 4.6 μM. Magnifications are 20× (panel A), 90× (panel B), and 40× (panel C). The length of the scale bars corresponds to 6 (panel A), 3 (panel B), and 4 μm (panel C).

the binding of H1 to acidic phospholipids (*19*−*22*). Intriguingly, we demonstrate here a pronounced increase in the secondary structure of H1 to be induced by the acidic phospholipid PS. More specifically, as indicated by the CD spectra H1 in aqueous solutions is a random coil, whereas the presence of PC/PS (8:2 molar ratio) vesicles significantly increases its contents of α-helicity and β-sheet structure, up to 7% and 24% (Table 1), respectively. Random coil structure was observed in the presence of PC vesicles (Figure 2). Accordingly, electrostatic interactions seem to be required for the phospholipid-induced alterations in the secondary structure of H1. A significant increment in α-helicity and β-sheet contents of H1 was observed also in trifluoroethanol. It is thus possible that also hydrophobic interactions could contribute in the phospholipid−H1 complex formation. We have previously demonstrated the formation of this complex to be associated with a significant increase in phospholipid acyl chain order, assessed from measurements on the steady-state emission anisotropy for the rodlike fluorophore diphenylhexatriene (*21*). To conclude, it is conceivable that efficient screening of the excess positive charges on the surface of H1 by the complexing acidic phospholipids together with lipid hydrocarbon−protein interactions causes the ordering of the protein. Our experiments further dem-

onstrate histone H1 to induce aggregation and fusion of liposomal membranes containing the acidic PS whereas only minor effects were observed for neutral SOPC liposomes. H1 may thus bind to adjacent PS-containing liposomes and cause their aggregation and fusion.

Following the above studies on the interaction of H1 with small vesicles, we proceeded to explore the macroscopic behavior of membrane-bound H1, together with histone H1 induced topological changes in liposomes. For this utility we employed so-called giant vesicles. The latter represent a novel biomembrane model, which has so far been used to investigate the physical properties of membranes (*42*), morphological changes such as fusion (*43*), and lipid lateral organization (*31*, *44*), as well as membrane interactions of DNA (*45*) and proteins (*46*). Giant vesicles have also been used to study the enzymatic modification of membrane lipids by phospholipases (*39*, *47*), low-density lipoprotein (LDL) (*38*), and sphingomyelinase (*48*, *49*). We have recently shown that antimicrobial peptides induce the formation of supramolecular peptide and lipid complexes, pinching off from the giant vesicle membranes and translocating into the aqueous cavity of the giant liposome (*32*, *33*). In the present study rapid binding of H1 microinjected on the surface of PS/PC giant liposomes was evident, and very small amounts of H1 (femtomoles, corresponding maximally to 0.2 pM H1 in the experimental system used) were enough to cause the observed topological changes in membranes. The membrane-bound histone H1 aggregated into patches, similarly to the mechanism of the "capping" of surface antigens as well as lipid cross-linking induced cap formation in cells (*50*, *51*). These aggregates then coalesced to form larger aggregates, followed by their internalization and shedding into the vesicle interior. In these experiments H1 was applied onto the giant vesicle surface by microinjection, causing a high local concentration. Local concentrations of H1 inside cells as well as in affected tissues could well be high. Recently, radiation-induced DNA double strand breaks were shown to release from chromatin significant amounts of H1 (up to 5−10% of the whole histone content in cells), which subsequently translocate into the cytoplasm (*52*). This H1 then interacts with mitochondrial membranes and induces permeability transition, releasing cytochrome *c* and triggering apoptosis. The outer mitochondrial membrane permeabilizing effect required similar concentrations (1.4−2.36 μM) as were used by us. In studies showing that extracellular matrix histone H1 bound to perlecan and induced myoblast proliferation, 0.014−2.36 μM protein was used (*7*). For therapeutic purposes 9.4 μM histone H1 was administered to leukemic T cells (*17*).

After the experiments with giant liposomes it was of interest to study the interactions of histone H1 with leukemic T cells and compare those with the macroscopic consequences observed in giant liposomes. Strikingly, the binding of TR-H1 to suspended cells as well as to individual cells positioned by holding them with a micropipet revealed very similar macroscopic patterns as observed for giant liposomes containing phosphatidylserine (Figure 9). Interestingly, except for the differences in macroscopic length scales of the aggregates this process seen in giant liposomes is virtually indistinguishable from the characteristic plasma membrane patterns of TR-H1 and the subsequent translocation of TR-H1 into the cytoplasm of these cells. In contrast to the punctate patterns of TR-H1 on PS-containing giant liposomes, homogeneous distribution of TR-H1 on SOPC liposomes was seen (data not shown), arguing for the involvement of PS in the association of histone H1 to the plasma membrane of leukemic T cells. Because of the high affinity of H1 to acidic phospholipids it is likely that this translocation is ATP-independent and driven by lipid phase changes induced by H1−PS complex formation, in keeping with a recent theoretical study by Harries et al. (*53*). Histone H1 is expected to cause the segregation of a domain of the negatively charged phospholipid, similarly to the results reported in studies on small vesicles (*21*). In this study, assuming (i) 60 Å^2 for the average area of a phospholipid and (ii) all microinjected H1 to become quantitatively associated with the giant liposome, the following estimates for H1:lipid stoichiometry (H1 per 1000 phospholipids, including lipids in both leaflets of the vesicle bilayer) were obtained, i.e., from 1.2 to 1.8 (Figure 4), from 11.5 to 29 (Figure 5B−F), from 4.7 to 12.2 (Figure 7), and 250 (Figure 10A). Binding of the acidic phospholipid to H1 would impose negative curvature for the protein-associated lipid surface. As a consequence of the screening of the charges of PS in the lipid−H1 interface, there is a decrease in the effective surface area in the contacting, external monolayer compared to the inner leaflet of the bilayer. Assuming the elastic energy for membrane bending to be less than the energy maintaining the 3-D structure of H1, this membrane condensation together with the negative curvature of the membrane underneath H1 and the aggregation of membrane-bound H1 would result in an endocytosis-like process, with the protein−membrane supramolecular complex translocating into the liposome. This process is thus somewhat analogous to that described for the internalization of ceramide-enriched microdomains following the enzymatic action of sphingomyelinase on giant liposomes, driven by lipid aggregation, area condensation, and bending rigidity (*31*, *48*, *49*). "Endocytosis" thus occurs upon relaxation of the system toward thermodynamic equilibrium. In this connection it is of interest that ceramide has been established to represent an apoptotic lipid messenger (*54*). It could be speculated that the induction of apoptosis in cells is triggered by vigorous lateral segregation of membrane constituents, with subsequent scrambling of part of the plasma membrane structures into cytoplasmic lipid−protein aggregates, resulting in the initiation of a large number of biochemical changes inside the cell, all aiming at disposing of the cell.

The composition of the leukemic T-cell plasma membrane certainly is much more complex than the SOPC/PS giant vesicles used here. However, it appears that the essential characteristics of the binding of H1 to T-cell plasma membrane are remarkably well reproduced by this simple model membrane, thus suggesting that the minimal requirements determining the macroscopic processes induced by H1 in Jurkat cells are satisfied by the SOPC/PS vesicles. This is not surprising in light of the very high affinity between H1 and PS, arising from an electrostatic attraction. Importantly, in tumor cells the lipid asymmetry is partially lost, and these cells thus expose the anionic phosphatidylserine on the external leaflet of their plasma membrane (*55*). Importantly, our data demonstrate that in the presence of the acidic phospholipid PS there is a major increase in the secondary structure of histone H1. In keeping with the

reported high affinity of H1 for acidic phospholipids (*19*−*21*), it is this exposed phosphatidylserine that is likely to bind histone H1. Moreover, this protein causes major changes in the PS-containing membranes in vitro and suggests PS-dependent structural changes of this protein to influence also its action on cells. Histone H1 binds to the plasma membrane of leukemic T cells and subsequently aggregates on the membrane, followed by the entry of this protein into the cells (*53*) and subsequent apoptosis. Class et al. suggested the cytotoxicity of H1 to be involved in its binding to a specific plasma membrane receptor (*17*). Although the involvement of a putative receptor cannot be excluded at this stage, our present data indicate that direct H1−PS interactions could be well sufficient. Interestingly, a recent report by Konishi et al. (*52*) reveals a key role for histone H1 in DNA damage-induced apoptosis. In brief, these authors showed that DNA double strand breaks due to radiation can induce translocation of nuclear H1 into the cytoplasm. Histone H1.2 in particular was found to be efficient in releasing cytochrome *c* from mitochondria. Importantly, the latter required very similar concentrations (micromolar) of H1 as used on suspension cells in our study. Yet, histone H1.2 did not show any direct interaction with Bcl-2 family members, and how this protein induces release of cytochrome *c* from mitochondria remains unknown. The authors speculated about lipid−histone interactions being involved. Our data certainly support this notion.

A number of proteins have been reported to aggregate on the surface of membranes containing acidic phospholipids, and polypeptide chains with β-sheet structure are extensively involved in amyloid fibril formation (for a review, see ref *56*). Interactions between misfolded proteins and lipids were suggested to play a role in the development of amyloid diseases (*57*). However, the molecular mechanisms underlying these interactions remain poorly understood. Similarly to histone H1, lysozyme, for example, is positively charged and has antibacterial activity (*58*), and this protein has been reported to form amyloid fibrils, this process being enhanced in the presence of negatively charged phospholipids (*59*, *60*). Intriguingly, multimeric complexes of α-lactalbumin and oleic acid have been found to induce apoptosis in tumor cells while the monomeric form of this protein was inactive (*61*−*63*). This complex caused apoptosis by inducing mitochondrial permeability transition with subsequent release of cytochrome *c* (*64*). A conformational change of α-lactalbumin oligomers toward a molten globule-like state has been suggested to be important for the translocation of this protein across phospholipid bilayers (*62*). The mode of translocation of α-lactalbumin thus resembles that observed for histone H1 aggregates (*63*). Aggregation of cationic proteins in the presence of negatively charged phospholipids, as well as the importance of lipid-induced protein conformational changes in their aggregation, may argue for a common mechanism. To this end, the above mechanisms appear to be closely parallel by that of the membrane structure perturbing antimicrobial peptides (*32*, *33*). Accordingly, the effects of histone H1 on leukemic T cells could involve the same mechanism in the triggering of apoptosis. The interesting range of consequences of the formation of the above supramolecular lipid−protein complexes, ranging from antibacterial action to amyloid formation and cytotoxicity, certainly warrants for detailed understanding of the involved molecular level processes.

ACKNOWLEDGMENT

The skillful technical assistance of Kaija Niva and Kristiina Söderholm is appreciated. The authors also thank Dr. Juha-Matti Alakoskela for stimulating discussions.

REFERENCES

1. Thomas, J. O. (1999) Histone H1: location and role, *Curr. Opin. Cell Biol. 11*, 312−317.
2. Ramakrishnan, V. (1997) Histone structure and the organization of the nucleosome, *Annu. Rev. Biophys. Biomol. Struct. 26*, 83−112.
3. Kubota, T., Kanai, Y., and Miyasaka, N. (1990) Interpretation of the cross-reactivity of anti-DNA antibodies with cell surface proteins: the role of cell surface histones, *Immunol. Lett. 23*, 187−194.
4. Emlen, W., Holers, V. M., Arend, W. P., and Kotzin, B. (1992) Regulation of nuclear antigen expression on the cell surface of monocytes, *J. Immunol. 148*, 3042−3048.
5. Mecheri, S., Dannecker, G., Dennig, D., Poncet, P., and Hoffman, M. K. (1993) Anti-histone autoantibodies react specifically with the B cell surface, *Mol. Immunol. 30*, 549−557.
6. Bolton, S. J., and Perry, V. H. (1997) Histone H1: a neuronal protein that binds bacterial lipopolysaccharide, *J. Neurocytol. 26*, 823−831.
7. Henriquez, J. P., Casar, J. C., Fuentealba, L., Carey, D., and Brandan, E. (2002) Extracellular matrix histone H1 binds to perlecan, is present in regenerating skeletal muscle and stimulates myoblast proliferation, *J. Cell Sci. 115*, 2041−2051.
8. Waga, S., Tan, E. M., and Rubin, R. L. (1987) Identification and isolation of soluble histones from bovine milk and serum, *Biochem. J. 244*, 675−682.
9. Raptis, L., and Menard, H. A. (1980) Quantitation and characterization of plasma DNA in normals and patients with systemic lupus erythematosus, *J. Clin. Invest. 66*, 1391−1399.
10. Brown, O. A., Sosa, Y. E., and Goya, R. G. (1997) Histones as extracellular messengers: effects on growth hormone secretion, *Cell Biol. Int. 21*, 787−792.
11. Czaja, A. J., Ming, C., Shirai, M., and Nishioka, M. (1995) Frequency and significance of antibodies to histones in autoimmune hepatitis, *J. Hepatol. 23*, 32−38.
12. Stemmer, C., Tuaillon, N., Prieur, A. M., and Muller, S. (1995) Mapping of B-cell epitopes recognized by antibodies to histones in subsets of juvenile chronic arthritis, *Clin. Immunol. Immunopathol. 76*, 82−89.
13. Wu, D., Ingram, A., Lahti, J. H., Mazza, B., Grenet, J., Kapoor, A., Liu, L., Kidd, V. J., and Tang, D. (2002) Apoptotic release of histones from nucleosomes, *J. Biol. Chem. 277*, 12001−12008.
14. Huggins, M. L., Todd, M. A., Cavers, S. R., Pavuluti, S. R., Tighe, P. J., and Powell, R. J. (1999) Antibodies from systemic lupus erythematosus (SLE) sera define differential release of autoantigens from cell lines undergoing apoptosis, *Clin. Exp. Immunol. 118*, 322−328.
15. Yasutomo, K. (2003) Pathological lymphocyte activation by defective clearance of self-ligands in systemic lupus erythematosus, *Rheumatology 42*, 214−222.
16. Richards, R. C., O'Neil, D. B., Thibault, P., and Ewart, V. (2001) Histone H1: an antimicrobial protein of atlantic salmon (*Salmo salar*), *Biochem. Biophys. Res. Commun. 284*, 549−555.
17. Class, R., Lindman, S., Fassbender, C., Leinenbach, H. P., Rawer, S., Emrich, J. G., Brady, L. W., and Zeppezauer, M. (1996) Histone H1 suppresses tumor growth of leukemia cells in vitro, ex vivo and in an animal model suggesting extracellular functions of histones, *Am. J. Clin. Oncol. 19*, 522−531.
18. Kleine, T. J., Lewis, P. N., and Lewis, S. A. (1997) Histone-induced damage of a mammalian epithelium: the role of protein and membrane structure, *Am. J. Physiol. 273*, C1925−C1936.
19. Periera, L. F., Marco, F. M., Boimorto, R., Caturla, A., Bustos, A., de la Concha, E. G., and Subiza, J. L. (1994) Histones interact with anionic phospholipids with high avidity; its relevance for the binding of histone-antihistone immune complexes, *Clin. Exp. Immunol. 97*, 175−180.

20. Koiv, A., Palvimo, J., and Kinnunen, P. K. J. (1995) Evidence for ternary complex formation by histone H1, DNA, and liposomes, *Biochemistry 34*, 8018−8027.
21. Rytömaa, M., and Kinnunen, P. K. J. (1996) Dissociation of cytochrome *c* from liposomes by histone H1. Comparison with basic peptides, *Biochemistry 35*, 4529−4539.
22. Subramanian, M., Jutila, A., and Kinnunen, P. K. J. (1998) Binding and dissociation of cytochrome *c* to and from membranes containing acidic phospholipids, *Biochemistry 37*, 1394−1402.
23. Bevers, E. M., Comfurius, P., and Zwaal, R. F. (1983) Changes in membrane phospholipid distribution during platelet activation, *Biochim. Biophys. Acta 736*, 57−66.
24. Kheiri, S. A., Fasy, T. M., and Billett, H. (1996) Effects of histones and a monoclonal autoantibody to H1 histones on clot formation in vitro: possible implications in the antiphospholipid syndrome, *Thromb. Res. 82*, 43−50.
25. Bahar, A. M., Kwak, J. Y. H., Beer, A. E., Kim, J. H., Nelson, L. A., and Beaman, K. D. (1993) Antibodies to phospholipids and nuclear antigens in nonpregnant women with unexplained recurrent abortions, *J. Reprod. Immunol. 24*, 220−222.
26. Cole, R. D. (1989). Purification and analysis of H1 histones, *Methods Enzymol. 170*, 524−532.
27. Wiedmer, S. K., Hautala, J., Holopainen, J. M., Kinnunen, P. K. J., and Riekkola, M.-L. (2001) Study on liposomes by capillary electrophoresis, *Electrophoresis 22*, 1305−1313.
28. Batzri, S., and Korn, E. D. (1973) Single bilayer liposomes prepared without sonication, *Biochim. Biophys. Acta 298*, 1015−1019.
29. Lakowicz, J. R. (1999) *Principles of fluorescence spectroscopy*, Kluwer Academic/Plenum Publishers, New York.
30. Andrade, M. A., Chaco'n, P., Merelo, J. J., and Mora'n, F. (1993) Evaluation of secondary structure of proteins from UV circular dichroism spectra using an unsupervised learning neural network, *Protein Eng. 6*, 383−390.
31. Holopainen, J. M., Angelova, M. I., and Kinnunen, P. K. J. (2000) Vectorial budding of vesicles by asymmetrical enzymatic formation of ceramide in giant liposomes, *Biophys. J. 78*, 830−838.
32. Zhao, H., Rinaldi, C. R., Di Giulio, A., Simmaco, M., and Kinnunen, P. K. J. (2002) Interactions of the antimicrobial peptides temporins with model membranes. Comparison of temporins B and L, *Biochemistry 41*, 4425−4436.
33. Zhao, H., Mattila, J. P., Holopainen, J. M., and Kinnunen, P. K. J. (2001) Comparison of the membrane association of two antimicrobial peptides, magainin 2 and indolicidin, *Biophys. J. 81*, 2979−2991.
34. Angelova, M. I., and Dimitrov, D. S. (1986) Liposome electroformation, *Faraday Discuss. Chem. Soc. 81*, 303−311.
35. Nelsestuen, G. L., and Lim, T. K. (1977) Equilibria involved in prothrombin- and blood-clotting factor X-membrane binding, *Biochemistry 16*, 4164−4171.
36. Matsuzaki, K., Nakayama, M., Fukui, M., Otaka, A., Funakoshi, S., Fujii, N., Bessho, K., and Miyajima, K. (1993) Role of disulfide linkages in tachyplesin-lipid interactions, *Biochemistry 32*, 11704−11710.
37. Tuominen, E. K., Wallace, C. J., and Kinnunen, P. K. J. (1997) The invariant ARG91 is required for the rupture of liposomes by cytochrome *c*, *Biochem. Biophys. Res. Commun. 238*, 140−142.
38. Duzgunes, N., Allen, T. M., Fedor, J., and Papahadjopoulos, D. (1987) Lipid mixing during membrane aggregation and fusion: why fusion assays disagree, *Biochemistry 26*, 8435−8442.
39. Holopainen, J. M., Angelova, M. I., Söderlund, T., and Kinnunen, P. K. J. (2002) Macroscopic consequences of the action of phospholipase C on giant unilamellar liposomes, *Biophys. J. 83*, 932−943.
40. Luisi, P. L., and Walde, P., Eds. (2000) *Giant vesicles*, John Wiley & Sons Ltd., Chichester, U.K.
41. Holopainen, J. M., Angelova, M., and Kinnunen, P. K. J. (2003) Giant liposomes in studies on membrane domain formation, *Methods Enzymol. 367*, 15−23.
42. Needham, D., and Zhelev, D. (2000) Use of micropipet manipulation techniques to measure the properties of giant lipid vesicles, in *Giant Vesicles* (Luisi, P. L., and Walde, P., Eds.) pp 103−147, John Wiley and Sons, Chichester, U.K.
43. Menger, F. M., and Lee, S. J. (1995) Induced morphological changes in synthetic giant vesicles: Growth, fusion, undulation, excretion, wounding, and healing, *Langmuir 11*, 3685−3689.
44. Korlach, J., Schwille, P., Webb, W. W., and Feigenson, G. W. (1999) Characterization of lipid bilayer phases by confocal microscopy and fluorescence correlation spectroscopy, *Proc. Natl. Acad. Sci. U.S.A. 96*, 8461−8466.
45. Angelova, M. I., Hristova, N., and Tsoneva, I. (1999) DNA-induced endocytosis upon local microinjection to giant unilamellar cationic vesicles, *Eur. Biophys. J. 28*, 142−150.
46. Fischer, A., Oberholzer, T., and Luisi, P. L. (2000) Corrigendum to Giant vesicles as models to study the interactions between membranes and proteins, *Biochim. Biophys. Acta 1467*, 177−188.
47. Dorovska-Taran, V., Wick, R., and Walde, P. (1996) A ^{1}H nuclear magnetic resonance method for investigating the phospholipase D-catalyzed hydrolysis of phosphatidylcholine in liposomes, *Anal. Biochem. 240*, 37−47.
48. Holopainen, J. M., Penate-Medina, O., Metso, A. J., and Kinnunen, P. K. J. (2000) Sphingomyelinase activity associated with human plasma low-density lipoprotein, *J. Biol. Chem. 275*, 16484−16489.
49. Nurminen, T. A., Holopainen, J. M., Zhao, H., and Kinnunen, P. K. J. (2002) Observation of topical catalysis by sphingomyelinase coupled to microspheres, *J. Am. Chem. Soc. 124*, 12129−12134.
50. Bretscher, M. S. (1984) Endocytosis: relation to capping and cell locomotion, *Science 224*, 681−686.
51. Hagiwara, H., Kogure, S., Nakamura, M., Shimada, Y., Ohno-Iwashita, Y., and Fujimoto, T. (1999) Cross-linking of plasmalemmal cholesterol in lymphocytes induces capping, membrane shedding, and endocytosis through coated pits, *Biochem. Biophys. Res. Commun. 260*, 516−521.
52. Konishi, A., Shimizu, S., Hirota, J., Takao, T., Fan, Y., Matsuoka, Y., Zhang, L., Yoneda, Y., Fujii, Y., Skoultchi, A. I., and Tsujimoto, Y. (2003) Involvement of histone H1.2 in apoptosis induced by DNA double-strand breaks, *Cell 114*, 673−688.
53. Harries, D., Ben-Shaul, A., and Szleifer, I. (2004) Enveloping of charged proteins by lipid bilayers, *J. Phys. Chem. B* (in press).
54. Pettus, B. J., Chalfant, C. E., and Hannun, Y. A. (2002) Ceramide in apoptosis: an overview and current perspectives, *Biochim. Biophys. Acta 1585*, 114−125.
55. Utsugi, T., Schroit, A. J., Connor, J., Bucana, C. D., and Fidler, I. J. (1991) Elevated expression of phosphatidylserine in the outer membrane leaflet of human tumor cells and recognition by activated human blood monocytes, *Cancer Res. 51*, 3062−3066.
56. Horwich, A. (2002) Protein aggregation in disease: a role for folding intermediates forming specific multimeric interactions, *J. Clin. Invest. 110*, 1221−1232.
57. Chauhan, A., Ray, I., and Chauhan, V. P. S. (2000) Interaction of amyloid beta-protein with anionic phospholipids: possible involvement of Lys^{28} and C-teminus aliphatic amino acids, *Neurochem. Res. 25*, 423−429.
58. Ibrahim, H. R., Higashiguchi, S., Juneja, L. R., Kim, M., and Yamamoto, T. (1996) A structural phase of heat-denatured lysozyme with novel antimicrobial action, *J. Agric. Food Chem. 44*, 1416−1423.
59. Adam, S., Higgins, A. M., and Jones, R. A. L. (2002) Surface-mediated folding and misfolding of proteins at lipid/water interfaces, *Langmuir 18*, 4854−4861.
60. Yonezawa, Y., Tanaka, S., Kubota, T., Wakabayashi, K., Yutani, K., and Fujiwara, S. (2002) An insight into the pathway of the amyloid fibril formation of hen egg white lysozyme obtained from a small-angle X-ray and neutron scattering study, *J. Mol. Biol. 323*, 237−251.
61. Hakansson, A., Zhivotovsky, B., Orrenius, S., Sabharwal, H., and Svanborg, C. (1995) Apoptosis induced by a human milk protein, *Proc. Natl. Acad. Sci. U.S.A. 92*, 8064−8068.
62. Svensson, M., Sabharwal, H., Hakansson, A., Mossberg, A. K., Lipniunas, P., Leffler, H., Svanborg, C., and Linse, S. (1999) Molecular characterization of α-lactalbumin folding variants that induce apoptosis in tumor cells, *J. Biol. Chem. 274*, 6388−6396.
63. Svensson, M., Hakansson, A., Mossberg, A. K., Linse, S., and Svanborg, C. (2000) Conversion of alpha-lactalbumin to a protein inducing apoptosis, *Proc. Natl. Acad. U.S.A. 97*, 4221−4226.
64. Köhler, C., Gogvadze, V., Hakansson, A., Svanborg, C., Orrenius, S., and Zhivotovsky, B. A. (2001) A folding variant of human alpha-lactalbumin induces mitochondrial permeability transition in isolated mitochondria, *Eur. J. Biochem. 268*, 186−191.

BI049758B